Copy No. 11

DEFENCE R&D DÉFENSE

MICROSTRUCTURAL CHARACTERIZATION AND ELECTRON, MICROPROBE ANALYSIS OF A NICKEL ALUMINUM BRONZE LASER-CLAD WELDMENT

J.A. Gianetto – R.Packwood – M. Sahoo

MATERIALS TECHNOLOGY LABORATORY

DEFENCE RESEARCH ESTABLISHMENT ATLANTIC

Contractor Report

DREA CR 1999-116

AUGUST 1999

National Defence Défense nationale

Canada

National Defence
Research and Development Branch

Défense nationale
Bureau de recherche et développement

DREA CR 1999-116

Microstructural Characterization and Electron Microprobe Analysis of a Nickel Aluminum Bronze Laser-Clad Weldment

J.A. Gianetto – R. Packwood – M. Sahoo

Materials Technology Laboratory
CANMET, NRCAN
568 Booth Street
Ottawa, Ontario, Canada
K1A 0G1)

Scientific Authority C.V. Hyatt

August 1999

CONTRACTOR REPORT

Prepared for

Defence Research Establishment Atlantic

Centre de Recherches pour la Défense Atlantique

Canada

102-03561/

ABSTRACT

In this study the microstructural and compositional variations that exist across a laser-clad weldment produced with a heat input of 150 J/cm and filler wire composition Cu-9.0% Al, 4.6% Ni, 3.9% Fe and 1.2% Mn were characterized. The weld metal, heat-affected zone and casting base metal structures and elemental distributions were evaluated using light optical microscope and electron microprobe, respectively. The results show that a considerable range of microstructures and some significant compositional variations are present in the laser-clad weldment investigated.

RÉSUMÉ

L'étude a permis de caractériser les changements de microstructure et de composition au sein d'un ensemble soudé plaqué au laser, obtenu grâce à une énergie thermique de 150 J/cm et à un fil d'apport de composition Cu-9,0 % Al, 4,6 % Ni, 3,9 % Fe et 1,2 % Mn. La structure et la distribution des éléments dans le métal fondu, dans la zone thermiquement affectée et dans le métal de base du moulage ont été déterminées à l'aide d'un microscope optique (dans le cas de la structure) et d'une microsonde électronique (pour la distribution des éléments). Les résultats révèlent une vaste gamme de microstructures et certaines variations importantes de composition dans l'ensemble soudé plaqué au laser qui a été analysé.

INTRODUCTION

The Defence Research Establishment Atlantic (DREA) has been conducting and sponsoring research on characterization and evaluation of laser surface melting and cladding of nickel aluminum bronzes (NAB) (1-9). NAB alloys are often used in marine applications including valve components and propulsion systems because of their high strength and good corrosion, erosion and cavitation resistance in seawater. In conjunction with this, it has been demonstrated that a low heat input laser-cladding method can be used as a cost-effective method for surface treatment of complex parts from ships and submarines.

Although a single phase martensitic structure can be produced under a relatively narrow range of laser welding heat inputs using a filler wire consumable electrode of composition (Cu-9.0 Al-4.6 Ni-3.9 Fe-1.2 Mn), further property improvements are being sought by focusing on the development of an optimal consumable alloy composition for cladding NAB components (8). The main goals are to have a cladding process that is less sensitive to heat input, and to produce laser cladding with improved properties including increased ductility. Several concurrent studies have been carried out to better understand the complex structures formed in the as-deposited and reheated weld metal regions of laser weld cladding (3-8). Owing to the complex microstructures and precipitation reactions that take place in NAB laser welds, characterization by TEM has been employed to identify the types of structures and to provide a better understanding of the transformation kinetics (4,8,9). The present investigation forms part of the overall effort to establish the structure/property relationships of NAB laser welds and ultimately provide better surface engineering processes and techniques for marine applications. As a result, the present study was undertaken to examine the range of structures and corresponding elemental distributions that exist in a relatively low heat input laser weld produced with a consumable electrode of composition Cu-9.0 Al-4.6 Ni-3.9 Fe-1.2 Mn.

EXPERIMENTAL PROCEDURES

AS-RECEIVED LASER CLAD NAB WELDMENT

The laser clad NAB weldment used in this investigation was supplied by DREA. The weldment was produced, under contract by the Laser Institute in Edmonton, and has been used in previous MTL and DREA studies. The laser operating conditions are shown in Table 1. A photograph of the laser weld clad surface is shown in Fig. 1, along with a schematic diagram and representative micrograph that shows the major regions of interest for this study. The laser cladding is composed of small overlapping weld beads, which form an alternating pattern of as-deposited and reheated weld metal regions, as shown in Fig. 1(b) and (c). In addition, heat

affected zone (HAZ) regions are formed in the casting substrate which must also be considered in evaluating the performance of a weldment.

The nominal composition of the substrate casting and laser weld metal, determined by spectrographic analysis, is listed in Table 2, along with the electrode wire composition (6).

METALLOGRAPHY AND MICROHARDNESS TESTING

Representative cross-sections of the as-received laser clad weldment were sectioned, mounted, and prepared using standard metallographic techniques. The specimens were etched in either a solution containing 50 mL ammonium hydroxide, 0.5 mL hydrogen peroxide and 50 mL distilled water, or an alcoholic ferric chloride solution. This allowed details of the weld metal regions, HAZ and base metal casting to be characterized using optical microscopy and microhardness surveys. The microhardness testing was performed using a diamond pyramid indenter with a 100 g load to facilitate measurements of specific microstructural regions.

ELECTRON MICROPROBE ANALYSIS

Bulk elemental analyses of specific regions and zones within the laser clad weldment were determined with a Cameca SX-51 microprobe using an accelerating voltage of 20 kV and beam currents of 10 to 30 nA. Specific regions of interest were identified and analyzed using either step (stage) or beam scans. The first analysis was carried out to determine the distribution of Al, Ni, Fe and Mn using a series of stage scans employing 1-μm steps with an accelerating voltage of 20 kV and beam current of 10 nA. In this case, individual scans were made across the as-deposited and reheated weld metal at a depth of ~100 μm from the clad surface. A through-thickness scan, beginning at the weld interface (fusion line) and traveling toward the surface, was also conducted. To acquire more detailed local concentration profiles, a series of short-stage scans were performed using the same 20 kV accelerating voltage, but with a 30 nA beam current. For these tests, an as-deposited region exhibiting a predominantly martensitic structure was analyzed for comparison with a mainly Widmanstatten α structure present in both the as-deposited and reheated regions. Local concentration profiles were also obtained for the dendritic structure near the weld fusion boundary, as well as across the HAZ/fusion boundary interface and a typical base metal region. Following a review of these preliminary analyses, it was decided that very short beam scans, using accelerating voltage of 10 kV and beam current of 10 nA, may reveal more about the elemental distribution in the mainly martensitic and Widmanstatten α lath-type structures.

RESULTS

MICROSTRUCTURE AND HARDNESS

The optical micrographs, presented in Fig. 2, show the representative regions observed in a typical cross-section of the laser-clad weldment. As previously mentioned, it has been shown that the laser-clad weldment is composed of a single (~0.5 mm thick) weld metal layer which has an alternating pattern of as-deposited (AD-dark regions) and reheated (RH-light bands) zones. Immediately beneath the weld metal are a narrow HAZ region and the unaffected base material. To understand the variation in microstructure across the laser weld cladding, further detailed examinations of the microstructural features were carried out at the four locations labeled A, B, C and D and correlated with microhardness measurements, as shown in Fig. 2. Several important trends are revealed from these data and the detailed microstructural features within specific regions. From the microhardness surveys, it is clear that significant variations in hardness exist across the weldment. This includes differences which depend on the microstructure formed in the as-deposited region - significantly lower hardness in the reheated weld metal regions, and a wide range of hardnesses in both the substrate HAZ and base metal casting. At the weld interface (fusion boundary), a relatively soft dendritic structure was frequently observed. In the as-deposited region, the dark etching areas have been classified as martensite (M) (>350 VHN) and are significantly harder than the adjacent Widmanstatten α (Wα) (260-297 VHN) regions. However, both regions are usually much harder than the adjacent reheated regions (<242 VHN) and this remains a concern with respect to the overall erosion and wear performance of this type of laser cladding.

In the following section, further details of the variations in weldment microstructure are described. At Location A in Fig. 2, a high proportion of martensite was formed in the as-deposited columnar region [Fig. 3(a) and (b)], whereas a predominantly Widmanstatten α structure was present in the reheated region [Fig. 3(c)]. In both regions, the prior β grain boundaries had narrow bands of allotriomorphic α decorating the respective columnar and equiaxed grains. At Location B, there was a clear transition in microstructure within the as-deposited region from mainly martensite existing near the fusion line, to a mixture of relatively fine Widmanstatten α with martensite towards the central (top) part of the weld bead [Fig. 4(a) and (b)]. This feature has been observed in previous studies as well as by other researchers who have studied laser welds in NAB (6-12). Again, allotriomorphic α delineates the prior β grain boundaries, and some dendritic solidification structure is observed, as indicated in Fig. 4(a). An interesting feature that has not been documented before can be see in the lower right-hand corner in Fig. 4(b). In this region, the predominantly martensitic structure has been etched in such a way as to reveal an underlying cellular dendritic structure. Most often the martensitic structure is revealed as a very fine lath-like structure, as shown in Fig. 3(b). This feature appears to be

related to a unique set of etching conditions. In Location C, (Fig. 5), a similar columnar structure was formed, however, the grain interior of this region exhibited a mixture of Widmanstatten α and martensite which resulted in an overall reduction in hardness (Fig. 2). Again, the reheated region was composed of Widmanstatten α structure, which exhibited a basket-weave morphology, as evident in Fig. 5(c). At Location D, shown in Fig. 6(a), there was a marked transition in microstructure from the fusion line to the weld surface. Initially a dendritic structure was formed, followed by very high hardness (404 VHN) martensite and finally Widmanstatten α. The light etching, high hardness martensite has very fine laths, as shown in Fig. 6(b).

The final microstructures to be examined were those of the substrate HAZ [Fig. 7(a)] and the base metal casting [Fig. 7(b)]. In comparing these structures, the effect of welding on the original base metal structure is evident. Figure 7(b) shows that the original base metal casting was composed of relatively coarse α grains with fine round κ_{IV} particles, lamellar eutectoid $\alpha + \kappa_{III}$ at the grain boundaries, and light and dark etching κ_{II} particles within or near the eutectoid phase. The HAZ [Fig. 7(a)], which underwent a partial retransformation to β, has on subsequent fast cooling transformed to martensite with some evidence of a eutectoid lamellar structure still remaining. The original α grains have elongated needle-like precipitates instead of the fine round κ_{IV} particles originally formed. Many relatively large κ_{II} precipitates are present, with some having been encapsulated in the weld metal near the fusion boundary [Fig. 7(a)].

ELECTRON MICROPROBE CONCENTRATION PROFILES

The first concentration profile was determined using a stage-scan across a complete weld bead, approximately 100 μm below the clad. In Fig. 8(a) the entire set of data is presented for Al, Ni, Fe and Mn. Figure 8(b) is a revised plot showing the average of every ten points, as well as the corresponding Ni/Fe ratio. It is important to note that the scan started at the fusion line of one bead and ended at the fusion line of the previous bead, so the first region to be analyzed was the reheated weld metal. As indicated, there was little change in Mn and synergistic variations in Al, Ni and Fe. Initially there was slightly lower Al, Ni and Fe, which subsequently rose and leveled off. The Al content was generally between ~7.0 and 8.0 wt %, while the Ni was between 4.5 and 5.0 wt % and Fe between 4.0 and 4.5 wt %. The Ni/Fe ratio did not change significantly, ranging from 1.04 and 1.11.

The results for the through-thickness scan, presented in Fig. 9, show variations in Al, Fe and Ni, as well as a table of the maximum, minimum, mean and standard deviation values. In this case, there was a larger variation in the Al content (about 7 to 9%) than for the horizontal scan presented in Fig. 8.

To determine if more insight into changes in concentration profiles could be detected for specific regions of the laser-clad weldment, a series of stage-scans was conducted using a higher beam current (30 nA). The results obtained from these analyses are presented in Figs. 10 to 12.

Figure 10(a) and (b) shows the location of a scan across an almost fully martensitic area in the as-deposited region of the laser-clad weld. The concentration profile corresponds to moving from position A to position B (80 μm long). In the SEM backscatter micrograph, it is clear that several prior β grain boundaries were intersected. Although synergistic variations in Al, Ni and Fe with relatively constant Mn were detected across the entire structure there was no significant changes even at the β grain boundaries. The compositional ranges of these elements are shown in Table 3.

Figure 11 shows the location and concentration profile obtained for a short scan across a predominantly Widmanstatten α structure in the as-deposited weld metal. Only small changes in composition are observed. Table 4 provides a comparison of these results and those obtained for a Widmanstatten α structure within reheated weld metal. In this particular case, the Widmanstatten α in the reheated region exhibits higher concentrations than in the as-deposited region.

The results obtained from a similar short scan across a predominantly dendritic-type structure is presented in Fig. 12(a) to (c). It is clear from the concentration profile that considerable compositional variation exists across the light regions of α and dark martensite. Major changes in Al, Fe and Mn are evident, including that as Al and Mn decrease Fe increases [Fig. 12(c)]. Towards the last half of the profile both Fe and Ni rise and fall together. Although it is clear that several dark and light regions were traversed it is difficult to precisely match these on the concentration profile. Therefore, the results were compared with those obtained from a much shorter scan (11 μm long) across a similar structure [Fig. 12(d)]. A summary of the results is included in Table 5. From this data it is clear that the light α phase has significantly lower levels of Al, as well as slightly lower Ni, Fe and Mn compared with the dark martensite phase.

In addition to the microprobe analysis of various weld metal regions, two stage-scans were carried out in selected areas near the HAZ/FL boundary and within the base metal casting. In both cases, very dramatic variations in composition were revealed. The optical and SEM micrographs (Fig. 13) show that the scan began in an α grain in the HAZ, traversed a eutectoid region and ended in the weld metal. A large κ_{II} particle, which was encapsulated in the weld metal, can be seen near the end of the scan. If one superimposes the concentration profile (Fig. 13) over these observed microstructural features, several interesting observations are revealed. First, there are significant changes in all but the Mn content which only increases in the large encapsulated κ_{II} particle. The marked variations in Al, Ni and Fe are accompanied by large variations in Cu. At the beginning of the scan in the α grain, there is relatively constant composition, while in the eutectoid region Ni-rich κ_{III} gobular and lamellar regions clearly contain high Ni with increased Fe and Al compared to the matrix. The Mn remains constant, except in the large κ_{II} particle. Very high Fe and correspondingly low Cu contents are character-

istic of this type of particle. In addition, it can be seen that high Ni and Al contents were found near the periphery of the particle. A summary of compositions is presented in Table 6.

The last area to be analyzed using a short stage-scan was a discrete region in the base metal casting (Fig. 14). In this location, the scan started in the α matrix and ran through a large κ_{II} particle then across a eutectoid α + κ_{III} region, ending in an adjacent α grain. This concentration profile is similar to the previous one (HAZ/FL) with the most pronounced change occurring at a large κ_{II} particle. A summary of these data is presented in Table 7.

In an attempt to gain more specific information about the compositional difference between a typical martensitic and Widmanstatten α lath-like structure, two short beam scans were made in the as-deposited region, as shown in Fig. 15. In this case, only Al and Fe were analyzed. For the lath-type structure, there was a parallel trend of decreasing then increasing Al and Fe [Fig. 15(d)] whereas, in the mainly martensitic region, there was more uniform Al with variation in Fe occurring at relatively wide lath boundaries [Fig. 15(e)]. If one compares the values listed in Table 8, some interesting trends emerge. In the lath-type structure, a clear pattern of alternating low and high levels of Al and Mn is observed, whereas in the martensitic structure there is less variation in Al with the Fe content varying by up to 1%.

DISCUSSION

The microstructural and compositional differences that exist across a laser clad NAB weldment produced with a heat input of 150 J/cm and filler wire consumable of composition Cu-9.0% Al, 4.6% Ni. 3.9% Fe and 1.2% Mn have been characterized. In general, the final weld deposit microstructure is dependent on the weld metal composition and thermal history, including the effects of reheating resulting from deposition of adjacent weld beads. In the HAZ region, the resultant structure depends, to a large extent, on the original casting microstructure and composition, and the thermal cycles experienced during welding (3,10-13).

MICROSTRUCTURE AND HARDNESS

There were significant microstructural and hardness variations within the laser-clad weldment investigated. In some areas of the as-deposited weld metal, a high proportion of relatively hard martensite was formed, while in other areas a mixture of Widmanstatten α and martensite or mainly Widmanstatten α was observed. In contrast, the reheated weld metal regions were composed mainly of Widmanstatten α. A transition from a columnar to more equiaxed structure was observed in going from the fusion boundary towards the central region of some weld beads. In addition, a relatively soft dendritic-type structure was frequently observed near the matrix fusion boundary. In both the as-deposited and reheated weld metal regions, the prior β grain boundaries were delineated by allotriomorphic α. These observations are in

agreement with those of other researchers who have studied laser welding of NAB castings (10-15).

Table 9 summarizes the microhardness of the various regions and structures observed in the laser-clad weldment. Clearly the predominantly martensitic regions exhibit the highest hardnesses - in excess of 350 VHN. The reheated regions vary between 236 to 242 VHN, which is much softer relative to the structures formed in the as-deposited region. An interesting feature, which was also observed in the as-deposited weld metal, was the dendritic-type structure that formed along the fusion boundary. The dendritic structure, which consists mainly of α with a dark etching phase formed along the interdendritic boundaries, displayed hardnesses below 200 VHN. A similar structure was observed by Marsico (14,15) in a laser-clad weld produced using a powder in place of a wire to clad NAB castings. The structure was composed of dendritic α and eutectoid reaction product, $\alpha + \kappa_{II}$ between dendrite arms. Martensite was rarely observed. The hardnesses of the two cladding processes were reported to be ~170 VHN for the powder laser weld and ~260 VHN for the wire laser weld, which are in close agreement with the present work.

In the substrate HAZ and casting base metal, a wide range of hardnesses was observed as a result of the microstructures present. In both the casting base metal and HAZ, lower hardnesses were associated with the large α grains, while high hardness levels corresponded to eutectoid regions which, in the case of the HAZ, had retransformed to β and on subsequent rapid cooling formed martensite. Although some studies have been published on the complex microstructures formed in the HAZ of NAB castings (3,10-13) there is more detailed information available on the structures formed in NAB castings (10,11,14,16-21).

COMPOSITIONAL VARIATION

The compositional variations that were detected by electron probe microanalysis of the various regions and structures of the laser-clad weldment are summarized in Table 10. Several trends emerge from review of these data. In the case of the weld metal region, the most significant findings are that the composition of the martensite and Widmanstatten α region within the as-deposited and reheated weld metal regions are similar and do not change appreciably over significant distances. Although the scan performed in the reheated region indicates that a slightly richer composition is displayed in this region, it is generally within the range observed for the as-deposited scans. These results are in general agreement with those from TEM studies performed on a similar laser-clad weld (4,9). The compositions of the as-deposited α and martensitic phases were comparable to the present results, with the exception of consistently lower Fe concentrations. This difference may be related to the high density of cuboidal precipitates that were present in both the α and martensitic phases.

One of the most pronounced compositional variations observed in the present study was associated with the dendritic-type structure that formed just inside the weld-fusion boundary. The formation of this type of structure is attributable to the leaner composition of the majority α phase. In most cases, the dendritic structure nucleated on the original α grains of the casting base metal. As indicated in Table 10, the α matrix has a relatively low Al concentration. In contrast, it should be noted that martensite tended to form in areas where the eutectoid structure was present along the fusion boundary. It is clear that this martensite has a higher concentration of Al (9.4%), with considerably higher Ni and Fe, than observed in martensitic regions within the weld bead. Since the laser weld bead is small and the transformation takes place so quickly there is insufficient time to allow complete mixing of the base metal casting and the filler wire near the fusion boundary. Thus, the major compositional gradient that exists in moving from the weld fusion boundary to the center of the bead accounts for the abrupt change in microstructure [Fig. 6(a)]. This is supported in part by another feature evidenced in this figure and also in Fig. 13. Clearly shown is the encapsulation of several κ_a particles just inside the fusion boundary. This suggests that there was insufficient time to completely dissolve the particles and little influence of turbulence since the particles were very close to the fusion boundary.

The microstructural and composition data obtained for the HAZ and casting base metal highlight the complexity of the NAB weldments. These results show that, in the case of the HAZ, the original casting composition and structure play a dominant role in the formation of the resultant HAZ microstructure.

SUMMARY

For the weld investigated, it would appear that the formation of either martensite or Widmanstatten α in the as-deposited region of the laser-clad weld is attributable to the marginally slower cooling time that is experienced towards the central portion of the weld bead and less to compositional differences. This is in agreement with earlier work (3), which showed that only a small increase in cooling time was needed to form Widmanstatten α instead of martensite in a Gleeble simulated NAB weld metal. Although no significant compositional differences were detected for the reheated regions of the laser-clad weld, the resultant structure is slightly coarser and considerably softer than those formed in the as-deposited region. In contrast, at locations near the fusion boundary inside the as-deposited region, a much more pronounced compositional difference was observed. The formation of a dendritic type structure was attributed to this difference and its nucleation and growth from the α grains in the HAZ, whereas martensite tended to be formed from the richer eutectoid structure. This inherent compositional gradient is considered responsible for the abrupt change in microstructure observed in going from the fusion boundary towards the center of the weld bead. The microstructural and

compositional data obtained for the HAZ and casting base metal highlight the complexity of the laser-clad NAB weldment.

ACKNOWLEDGMENTS

The authors wish to thank Dr. C. Hyatt, Defence Research Establishment Atlantic for supplying the laser-clad NAB weld used for this investigation and for many enlightening discussions throughout the course of this collaborative work. They also appreciate the technical assistance provided by Ms. C. Bibby in preparing samples for metallographic examination. They thank Dr. G. McMahon for technical reviewing and comments on this report.

REFERENCES

1. Magee, K.H. "Laser surface modification and cladding of nickel aluminum bronze", Contractor Report for Defence Research Establishment Atlantic, DREA CR/93/421, 1993.
2. Hyatt, C.V. and Magee, K.H. "Laser surface melting and cladding of nickel aluminum bronzes", Int. Conf. on Advanced Joining Technologies for New Materials II, AWS, Cocoa Beach, FL, pp. 111-126, 1994.
3. Gianetto, J.A., Sahoo, M., Letts, M.W. and Bibby, C. "Microstructural characterization of NiAl bronze weldments", Metal Technology Laboratories-CANMET Report: MTL 95-03(TR-R), DREA CR/95/435, 1995.
4. Bennet, J.C. "Microstructural characterization of laser-clad nickel aluminum bronze alloys by transmission electron microscopy", DREA CR/96/442, Defence Research Establishment Atlantic, Dartmouth, Nova Scotia, 1996.
5. Hyatt, C.V. "Review of literature related to microstructural development during laser surface engineering of nickel aluminum bronze", Technical Memorandum 96/227, DREA, Defence Research Establishment Atlantic, Dartmouth, Nova Scotia, 1997.
6. Hyatt, C.V., Magee, K.H. and Betancourt, T. "Effect of heat input on the microstructure and properties nickel aluminum bronze laser clad with a consumable of composition Cu-9.0Al-4.6Ni-3.9Fe-1.2Mn", Submitted for publication in Metall. Trans., 1997.
7. Hyatt, C.V., Gianetto, J.A., Bennet, J.C., Sahoo, M., Letts, M.W. and Bibby, C. "Simulation of microstructures in laser clad nickel aluminum bronzes", Proc. of 6th Int. Conf. on Welding and Melting by Electron and Laser Beams,.CISFFEL, Paris, France, 1998.
8. Hyatt, C.V., Bennet, J.C., Pelletier, G., KarisAllen, K., Hewitt, J., Gianetto, J.A. and Sahoo, M. "Development of an optimum consumable alloy for low heat input welding of nickel aluminum bronzes", Proc. of 3rd CF/CRAD Meeting on Naval Applications of Materials Technology, Defence Reseach Establishment Atlantic, Halifax, Nova Scotia, April, 1997.

9. Bennet, J.C. and Hyatt, C.V. "Microstructural characterization of laser-clad nickel aluminum bronze alloys by TEM", Proc. of 3rd CF/CRAD Meeting on Naval Applications of Materials Technology, Defence Reseach Establishment Atlantic, Halifax, Nova Scotia, pp. 321-339, April, 1997.
10. Bell, D.E., Marsico, T.A., Petrolonis, K., Denny, P.E. and Howell, P.R. "The microstructure of laser welded aluminum bronzes", Proc.of Metallography: Past, Present and Future, ASTM STP 1165, Eds. G.F. Vander Voort, F.J. Warmuth, S.M. Purdy and A. Szirmae, American Society for Testing of Materials, Philadelphia, pp. 327-343, 1993.
11. Bell, D.E., Petrolonis, K. and Howell, P.R. "Solid-solid phase transformations in laser welded aluminum bronzes", Conf.Proc. on Int. Trends in Welding Science and Technology, ASM International, Gatlinburg, TN, Eds. S.A. David and J.M. Vitek, pp. 301-305, 1992.
12. Petrolonis, K. "Laser surface welded nickel aluminum bronze (Cu-9 Al-4 Fe-4 Ni)", Welding Journal, Vol. 72, No. 7, pp. 301s-306s, 1993.
13. Marsico, T.A., Bell, D.E., Petrolonis, K. and Howell, P.R. "Microstructural development in metal inert gas and laser beam welded nickel aluminum bronze", Proc.of Annual TMS Meeting on Laser Processing-IV, Feb. 1993, Denver, CO, Minerials, Metals and Materials Society (TMS), Warrendale, PA., pp. 191-202, 1994.
14. Marsico, T.A. "Microstructural development in cast and laser beam clad nickel aluminum bronze", PhD Thesis, The Pennsylvania State University, 1996.
15. Marsico, T.A. "Laser processing of nickel aluminum bronze for use in propeller fabrication and repair", Proc. of 3rd CF/CRAD Meeting on Naval Applications of Materials Technology, Defence Reseach Establishment Atlantic, Halifax Nova Scotia, pp. 299-320, April, 1997.
16. Sahoo, M., Edwards, J.O. and Thomson, R. "Influence of corrosion inhibiting heat treatment on the microstructure and mechanical properties of nickel-aluminum bronze alloy C95800", Trans. of American Foundrymen's Society, Vol. 87, pp. 495-502, 1979.
17. Sahoo, M., Edwards, J.O. and Thomson, R. "Influence of corrosion inhibiting heat treatment on the microstructure and impact properties of nickel-aluminum bronze alloy C95800", Trans. of American Foundrymen's Society, Vol. 88, pp. 769-776, 1980.
18. Brezina, P. "Heat treatment of complex aluminum bronzes", Int. Metals Review, Vol. 27, pp. 77-120, 1982.
19. Hason, F., Jahanafrooz, A., Lorimer, G.W. and Ridley, N. "The morphology, crystallography, and chemistry of phases in as-cast nickel-aluminum bronze", Metall. Trans., Vol. 13A, No. 8, pp. 1337-45, 1982.
20. Jahanafrooz, A., Hason, F., Lorimer, G.W. and Ridley, N. "Microstructural development in complex nickel-aluminum bronzes", Metall. Trans., Vol. 14A, No. 10, pp. 1951-56, 1983.
21. McMahon, G., Gianetto, J.A. and Sahoo, M.A. "Microstructural characterization of sand-cast Ni-Al Bronzes", Materials Technology Laboratory - CANMET Report, MTL 97-02(TR-R), 1997.

Table 1 - Laser weld cladding conditions.

Specimen ID	Power W	Travel speed mm/s	Wire dia. mm	Defocus mm	Shielding gas	Heat input J/mm
A150/1	3300	21	0.25	10.2	Ar	150

Table 2 - Chemical composition of NAB materials.

Specimen	Designation	Element (wt %)			
		Al	Ni	Fe	Mn
Casting	C95800	8.6	4.7	4.5	1.6
Wire	ER CuNiAL	9.0	4.6	3.9	1.2
Laser Weld	A150/1	8.7	4.7	4.5	1.5

Table 3 - Compositional range of martensitic region in the laser weld.

Martensite	Element wt %			
	Al	Ni	Fe	Mn
Range	~7.9-8.8	4.5-5.0	4.0-4.5	~1.5

Table 4 - Compositional range of Widmanstatten α structure in the laser weld.

Region	Element wt %			
	Al	Ni	Fe	Mn
As-deposited				
Range	7.41-8.44	4.33-5.01	3.97-4.56	1.50-1.72
Avg.	8.05	4.73	4.41	1.63
Reheated				
Range	7.96-9.33	4.74-5.57	4.67-5.48	1.62-1.83
Avg.	8.61	5.32	5.06	1.75

Table 5 - Compositional range of dendritic structures near the interface fusion boundary in the laser weld.

Scan	Position	Element wt %			
		Al	Ni	Fe	Mn
Fig. 12(c)	Range	6.66-8.94	3.28-3.95	2.27-3.48	1.38-2.36
	11 μm	7.01	3.83	3.34	1.42
	14 μm	8.94	3.69	2.54	2.35
	26 μm	6.79	3.81	3.30	1.38
	40 μm	8.31	3.62	2.58	2.26
Fig. 12(d)	Point # /Phase				
	Range	7.04-11.00	3.38-4.54	3.31-4.61	1.21-1.87
	2-light	7.63	3.56	3.42	1.61
	5-dark	11.00	4.45	4.13	1.84
	9-light	7.49	4.06	4.55	1.21
	15-dark	10.24	4.32	4.50	1.78
	19-light	8.02	3.41	3.50	1.52

Table 6. - Compositional variation in HAZ/FL region.

Region	Location	Element wt %			
		Al	Ni	Fe	Mn
α matrix	Beginning of scan	7.28-8.07	3.17-3.97	2.16-4.62	1.60-1.82
eutectoid	#1 globular	10.79	7.85	7.03	1.90
$\alpha + \kappa_{III}$	#2 globular	12.65	11.49	5.98	2.00
	#3 lamellar	10.82	10.91	7.85	2.01
	#4 globular	11.42	11.98	11.52	2.00
	#5 lamellar	11.06	6.36	11.17	1.91
		12.02	8.51	14.81	1.97
		10.99	7.03	11.50	1.82
weld metal	(65-85 μm)	8.36-9.61	4.68-7.01	2.99-6.01	1.63-1.93
large κ_{II}	near edge	12.83	16.44	15.59	2.17
particle	near center	11.17	9.79	62.03	3.79
~7.5 μm dia.	near center	10.94	9.62	62.67	4.31
	near edge	11.04	10.91	12.94	1.70
weld metal	End of scan near FL	9.41	7.59	5.67	1.50

Table 7 - Compositional variation in base metal casting region.

Region	Location	Element (wt %)			
		Al	Ni	Fe	Mn
α matrix	1-8 μm	7.41-7.93	3.11-4.17	2.90-5.63	1.64-1.77
(avg.)		7.66	3.79	3.86	1.73
large κ_{II}	near edge	5.54	4.12	44.69	7.62
particle	near center	5.46	4.93	65.47	9.55
~10 μm dia.	near center	7.63	7.03	59.36	7.19
	near edge	12.11	12.37	31.59	3.23
	Total (20-36 μm)	8.07-10.22	3.53-7.83	3.26-7.21	1.61-1.91
	(avg.)	9.07	5.62	4.64	1.77
eutectoid	23 μm	9.43	6.79	4.88	1.77
$\alpha + \kappa_{III}$	33 μm	10.21	7.83	7.21	1.91
	35 μm	9.41	6.15	5.77	1.80
α grain	(37-47 μm)	7.13-7.98	2.59-3.32	1.63-2.67	1.52-1.71
	(avg.)	7.63	2.87	2.07	1.65

Table 8 - Compositional variation in as-deposited weld metal region using short beam scans.

Region	Location	Element wt %	
		Al	Fe
Lath-type	Range	7.65-9.54	3.48-4.72
	Avg.	8.55	4.12
	Low Al	7.67	3.61
	High Al	9.28	4.34
	Low Al	7.65	3.56
	High Al	9.55	4.32
	Low Al	8.25	3.98
Martensite	Range	8.16-9.12	3.39-5.03
	Avg.	8.63	4.18
	Points 3-6	8.90	4.81
	Points 9-18	8.43	3.70
	Points 20-22	8.67	4.56

Table 9 - Summary of microhardness for different regions and structures in the laser-clad weldment.

Location*	Region/Structure	Microhardness, VHN_{100}
A	As-deposited/Martensite	354
	As-deposited/Widmanstatten α	297
	Reheated	238
	Dendritic	184
B	As-deposited/Martensite	353
	As-deposited/Widmanstatten α	260
	Reheated	236
C	As-deposited/ Martensite + Widmanstatten α	281
	Reheated	242
D	As-deposited/Martensite	338-409
	As-deposited/Widmanstatten α	280
HAZ	HAZ near the fusion line	236 (150-343)
Base Metal	Casting Base Metal	161 (128-207)

*See Fig. 2

Table 10 - Summary of compositional variation in the laser weldment.

Regions	Element wt %			
	Al	Ni	Fe	Mn
Weld metal				
As-deposited martensite	7.9-8.8	4.5-5.0	4.0-4.5	1.5
As-deposited Widmanstatten α	8.1	4.7	4.4	1.6
Reheated Widmanstatten α	8.6	5.3	5.1	1.8
Dendritic Structure Area #1				
α	~6.8	3.8	3.3	~1.4
dark etching phase	8.3-8.9	3.6	2.5	2.3
Dendritic Structure Area #2				
α	7.5	3.6-4.0	3.4-4.5	1.2-1.6
dark etching phase	10-11	4.3-4.4	4.1-4.5	~1.8
HAZ/FL				
α matrix	7.3-8.1	3.2-4.0	2.2-4.6	1.6-1.8
eutectoid α + κ_{III}	10.8-11.0	7.8-12.0	7.0-11.5	1.9-2.0
κ_{II} particle in weld metal	11.0	9.6	62.7	4.3
weld metal martensite	9.4	7.6	5.7	1.5
Base Metal				
α matrix	7.7	3.8	3.9	1.7
eutectoid α + κ_{II}	10.2	7.8	7.2	1.9
κ_{II} particle	5.5	4.9	65.5	9.6
α matrix	7.6	2.9	2.1	1.6

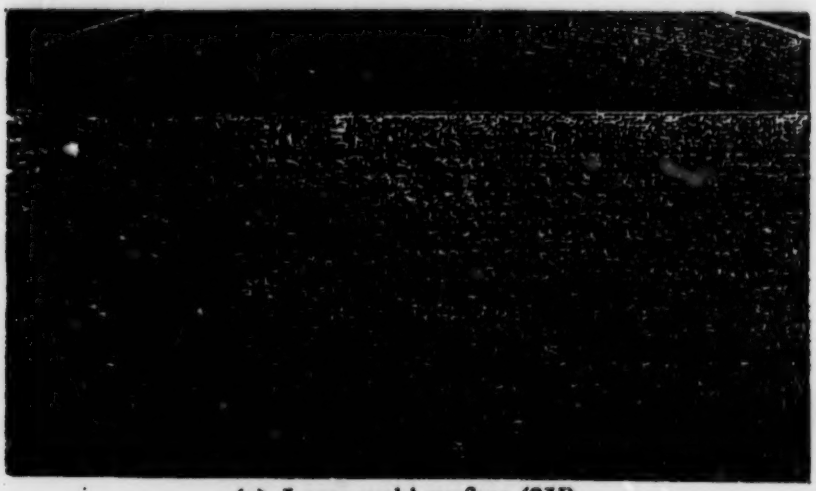

(a) Laser weld surface (2X).

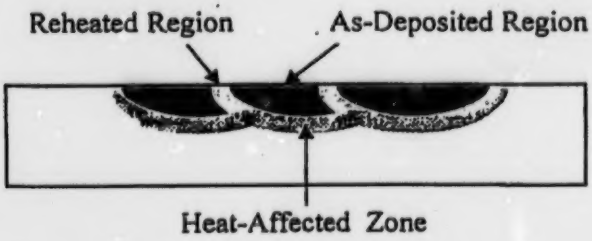

(b)

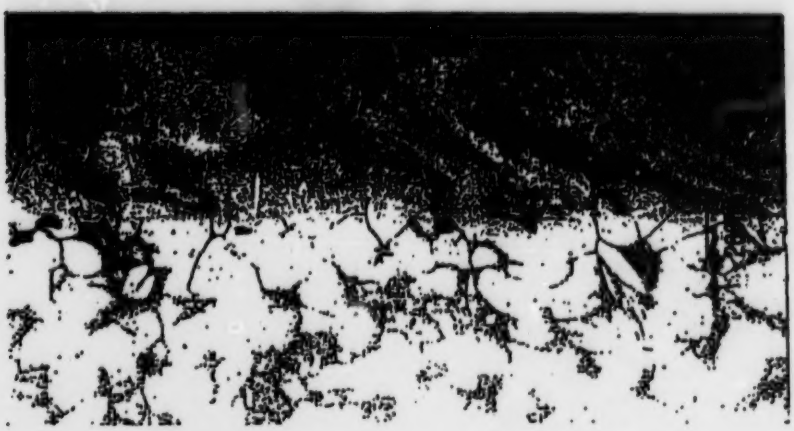

(c)

Fig. 1. Photograph, schematic diagram and optical micrograph of laser-clad weldment.

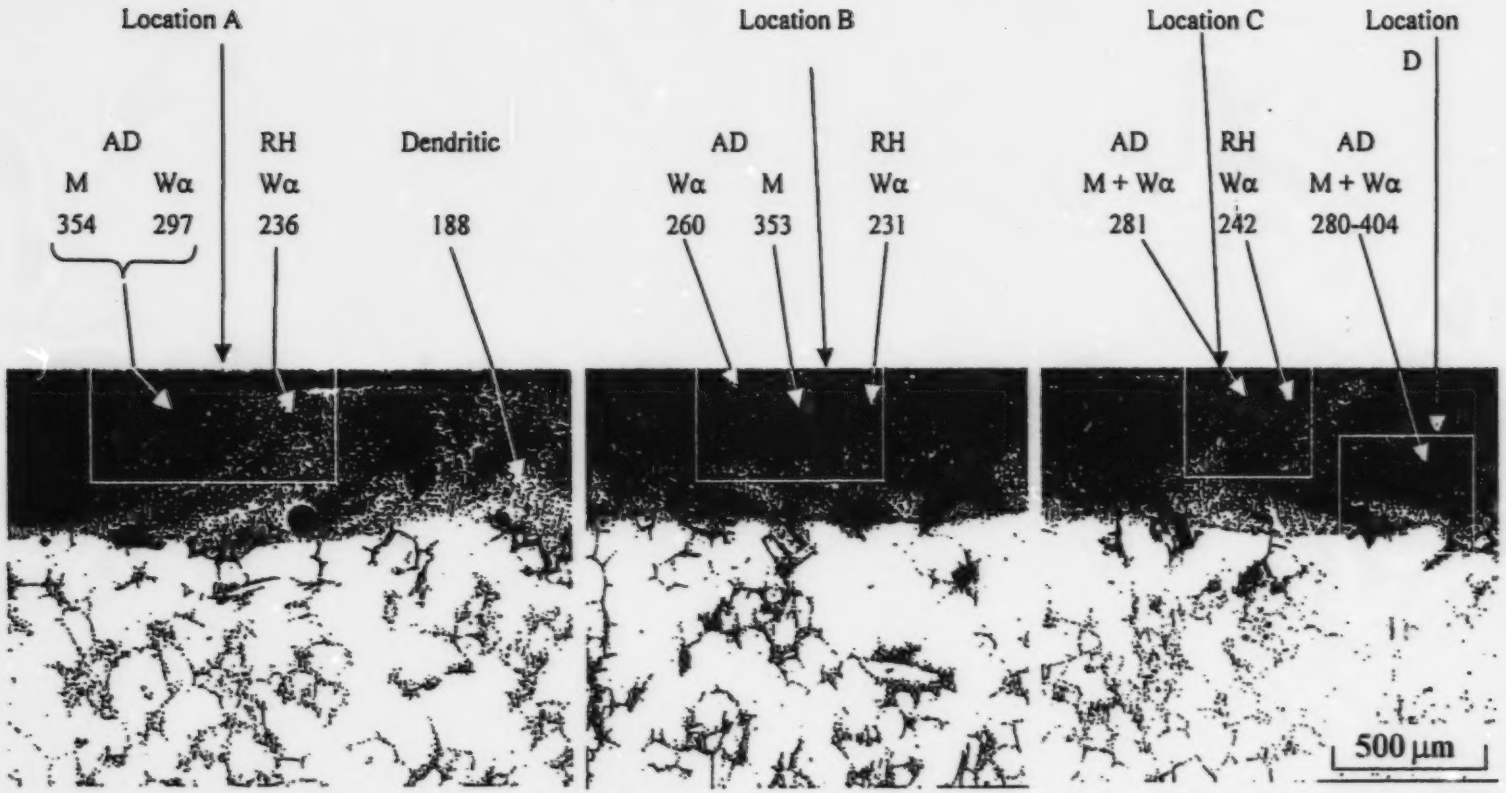

Fig. 2. Optical micrographs showing representative cross-section of laser-clad weldment and location of microhardness (VHN) measurements. AD = as-deposited, RH = reheated, HAZ = heat-affected zone, M = martensite, and Wα = Widmanstatten α.

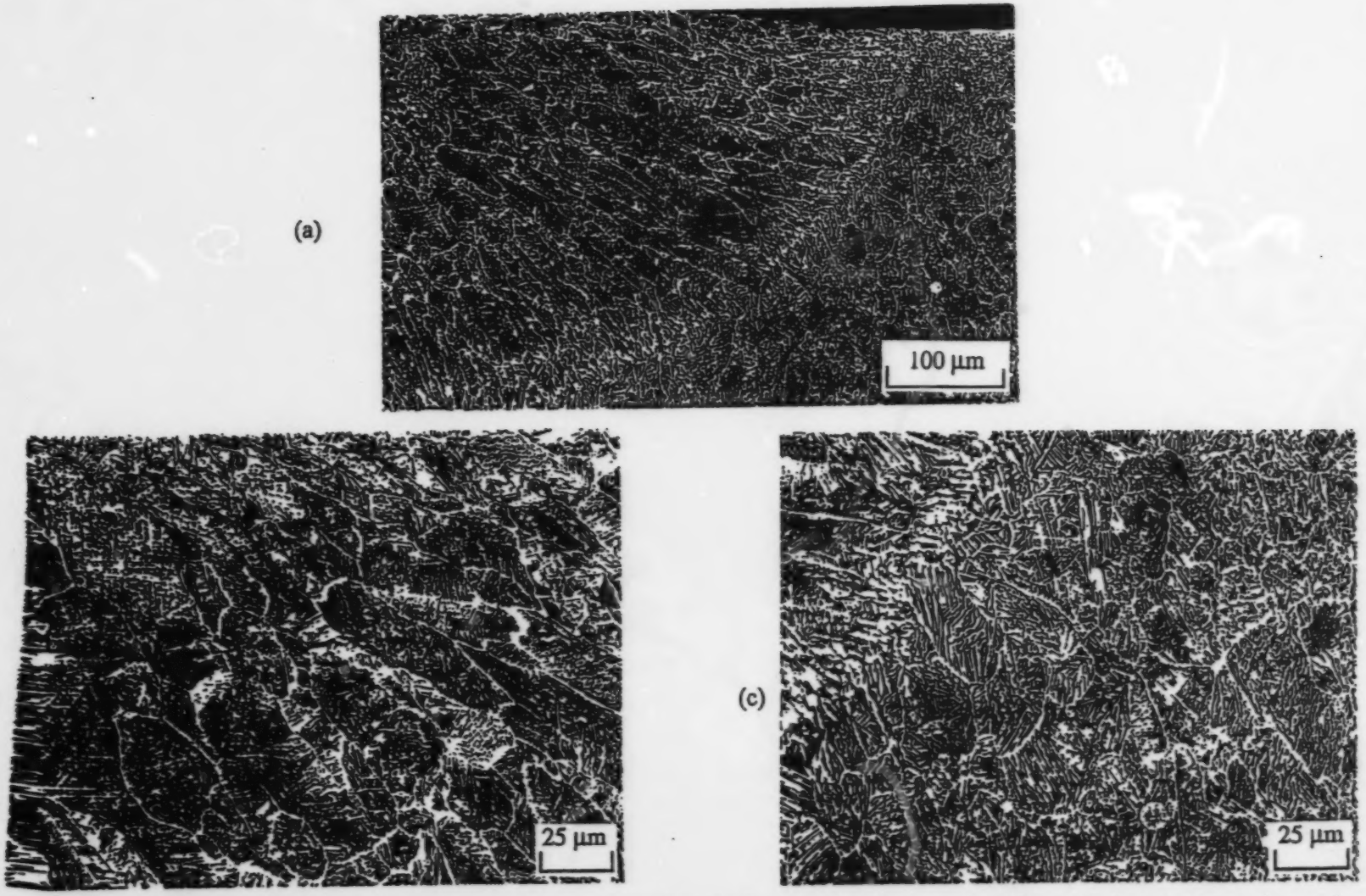

Fig. 3. Optical micrographs showing (a) overview of columnar as-deposited and equiaxed reheated weld metal microstructures observed at Location A in Fig. 2, (b) as-deposited structure consisting mainly of martensite with prior β grain boundaries delineated by allotriomorphic α, and (c) reheated weld metal with equiaxed prior β grains and a mainly Widmanstatten α microstructure.

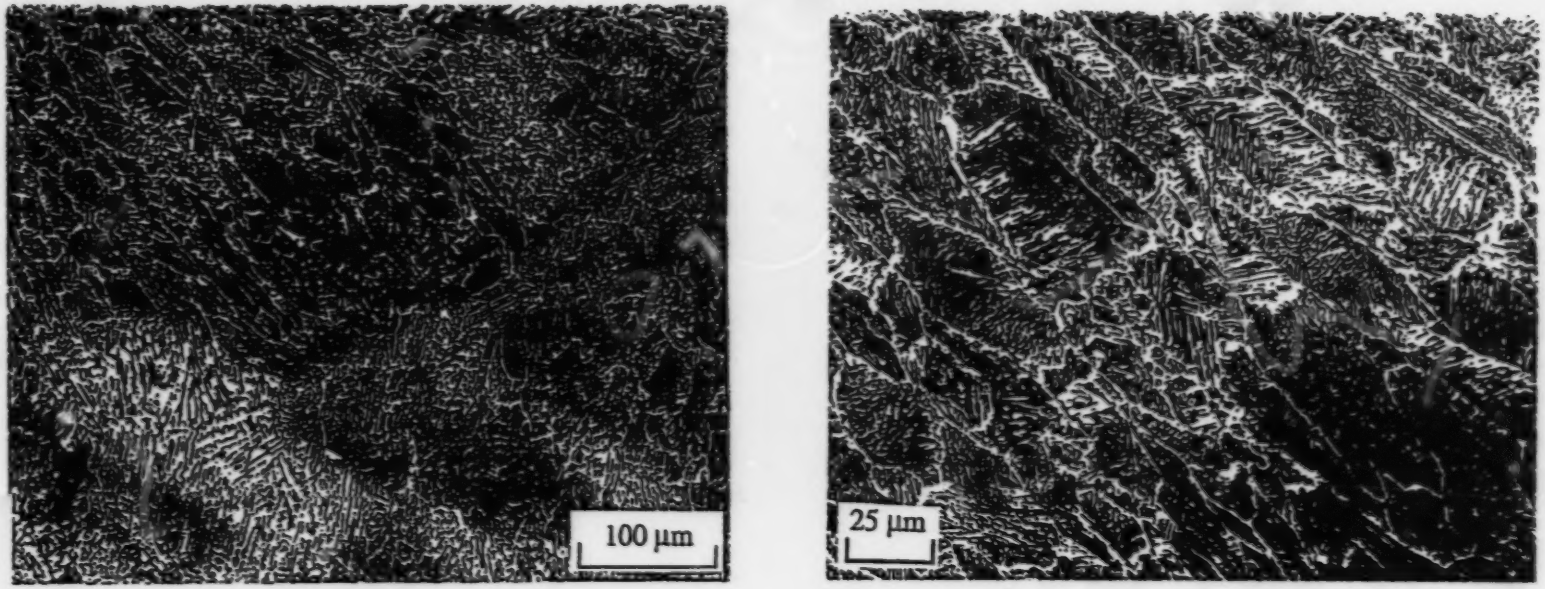

(a) (b)

Fig. 4. Optical micrographs showing (a) the transition from mainly martensite near the fusion boundary to a predominantly Widmanstatten α microstructure towards the central region of the weld bead at Location B, (b) detail of Widmanstatten α structure with some martensitic regions and prior β grain boundaries delineated by allotriomorphic α.

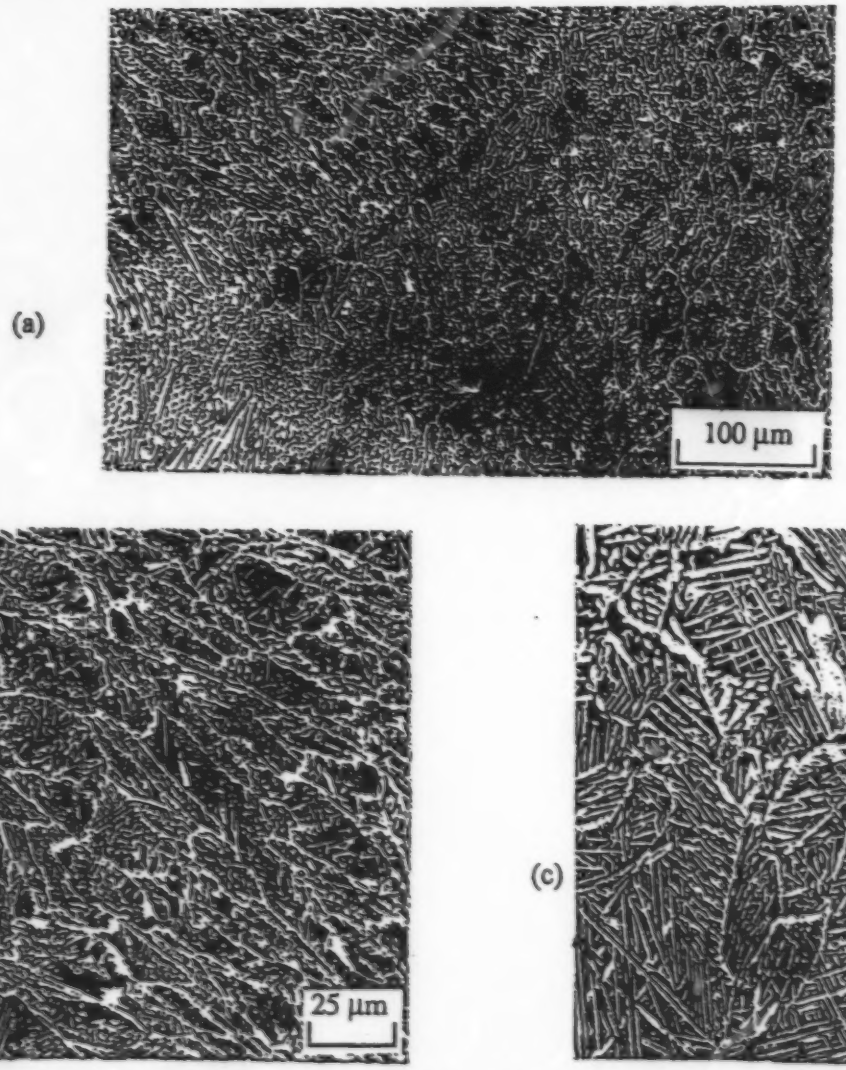

Fig. 5. Optical micrographs showing (a) overview of columnar as-deposited and equiaxed reheated weld metal microstructures observed at Location C in Fig. 2, (b) as-deposited structure composed of Widmanstatten α (light lath-like areas) with fragmented regions of martensite (dark areas), and (c) reheated weld metal with equiaxed prior β grains and Widmanstatten α with lath-like or basket-weave morphologies.

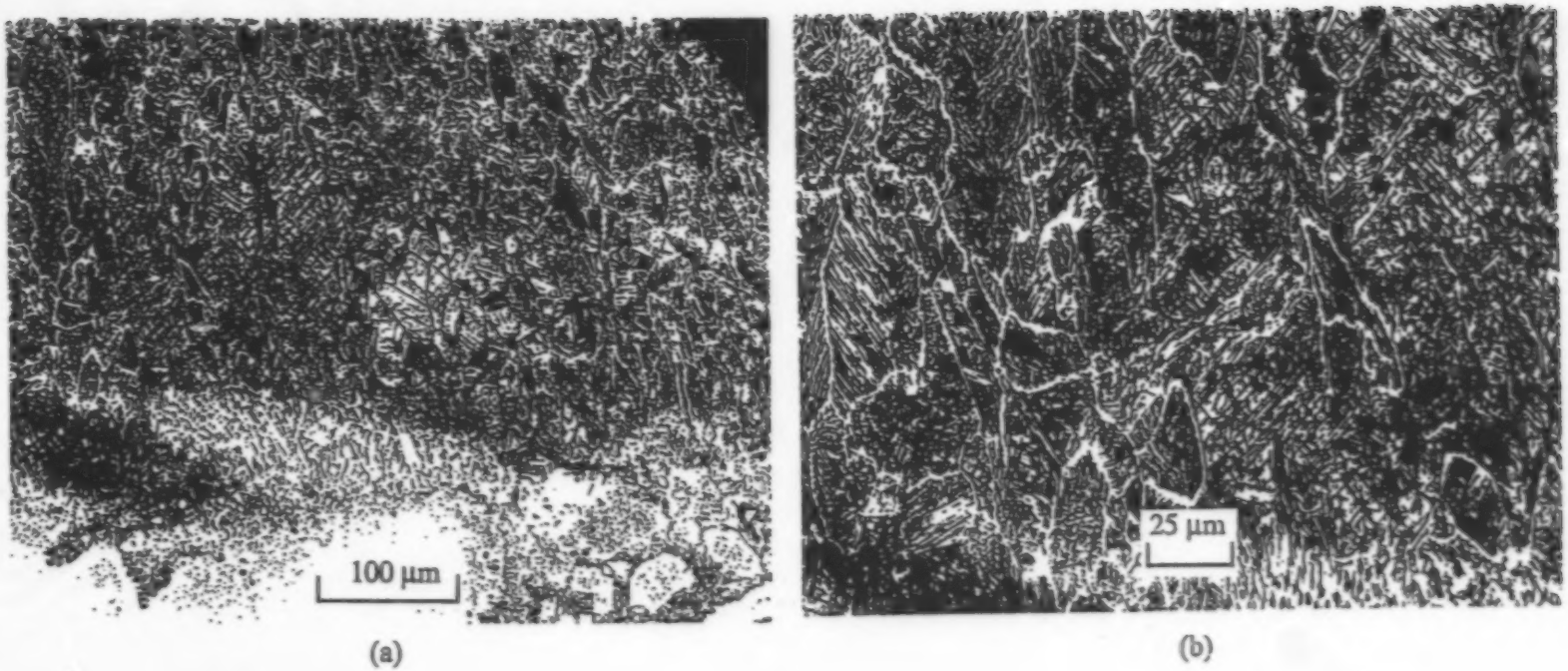

Fig. 6. Optical micrographs showing (a) the transition from a dendritic to columnar as-deposited structure consisting mainly of martensite to a Widmanstatten α microstructure towards the central (top) region of the weld bead at Location D in Fig. 2 and (b) detail of high hardness martensitic structure with very fine laths and prior β grain boundaries delineated by allotriomorphic α.

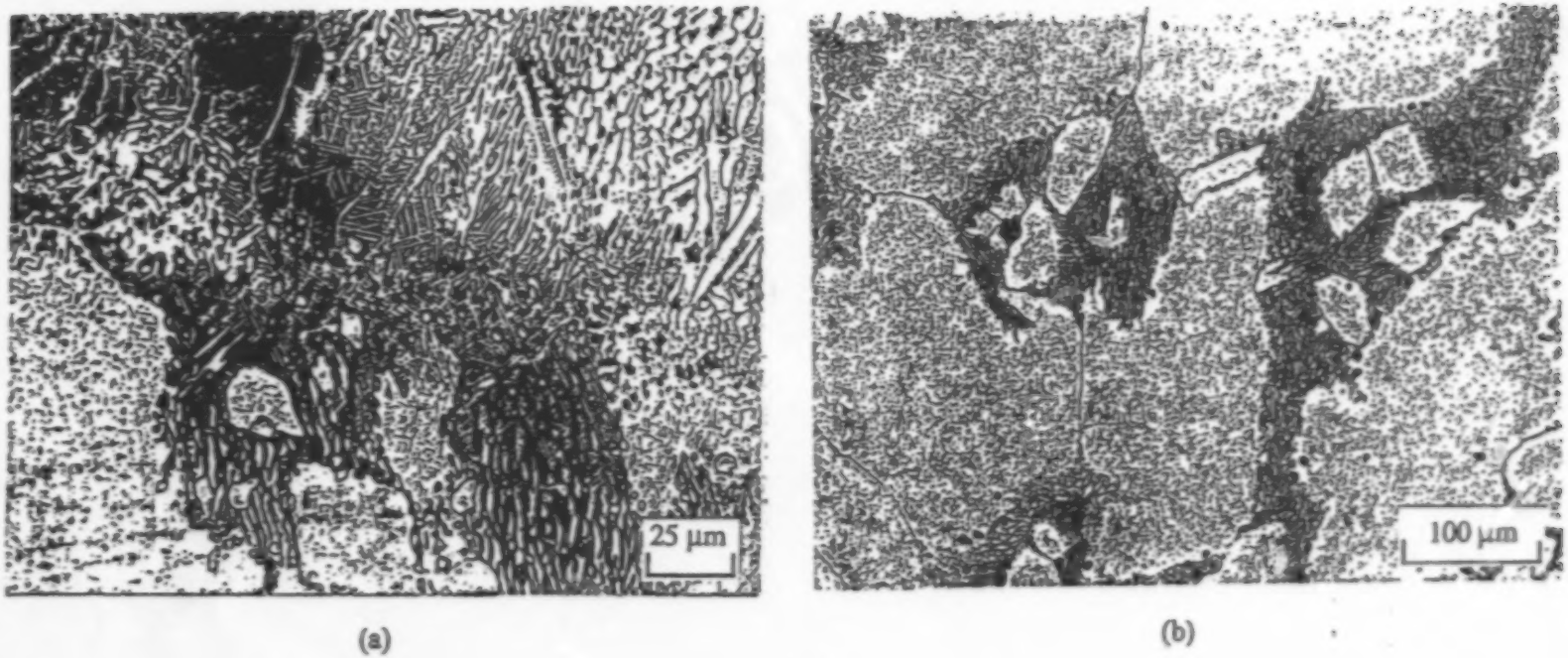

(a) (b)

Fig. 7. Optical micrographs showing (a) representative structure of the substrate HAZ observed near the fusion boundary. Original α grains with elongated plate-like κ precipitates and high hardness martensite (dark areas) with relatively large κ_{II} particles is observed and (b) casting substrate microstructure with coarse a grains which contain small κ_{IV} particles, eutectoid lamellar α + κ_{III} at grain boundaries and triple points as well as larger κ_{II} iron-rich precipitates superimposed or in the vicinity of the lamellar regions.

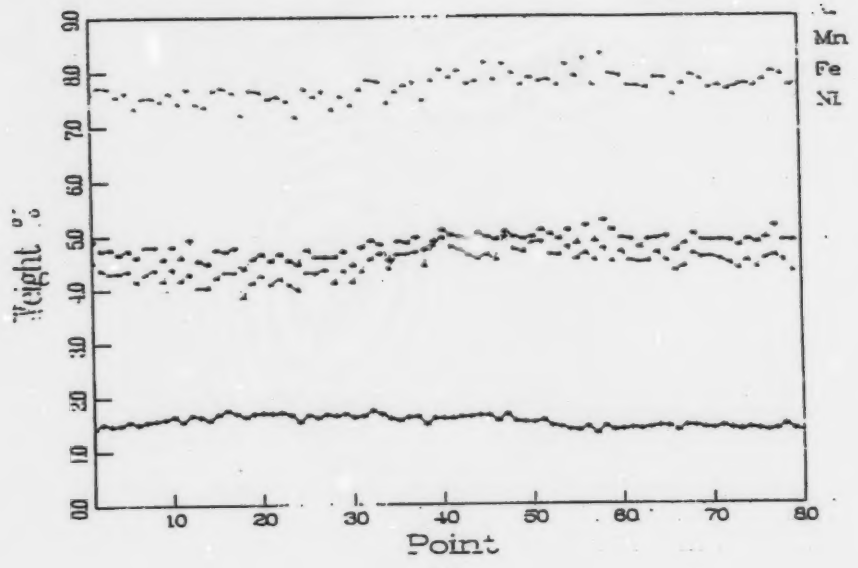

(a)

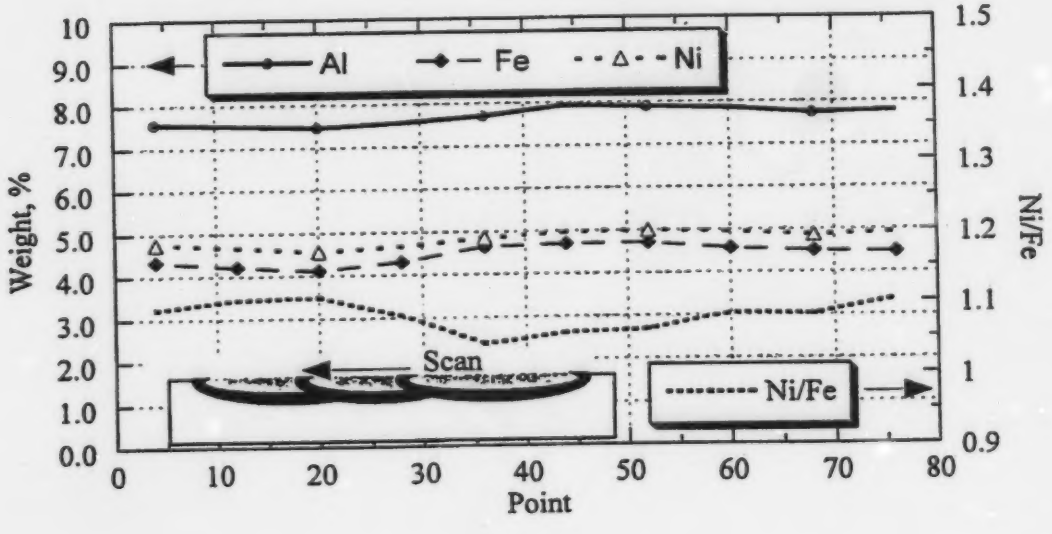

(b)

Fig. 8. Concentration profiles for horizontal stage-scan from fusion boundary to fusion boundary.

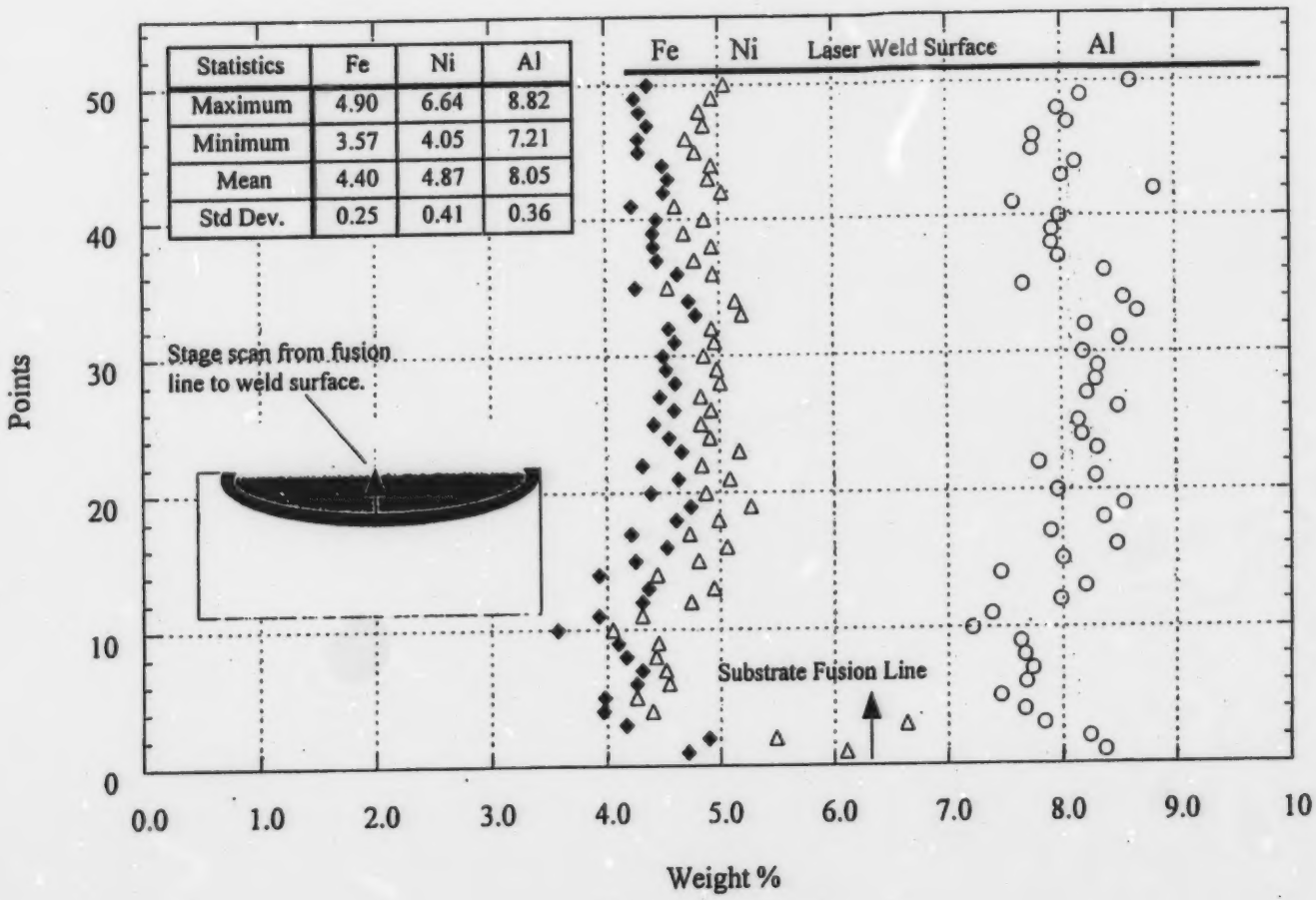

Fig. 9. Concentration profile for a through-thickness stage-scan beginning at the fusion boundary and traversing towards the surface of the laser clad weldment.

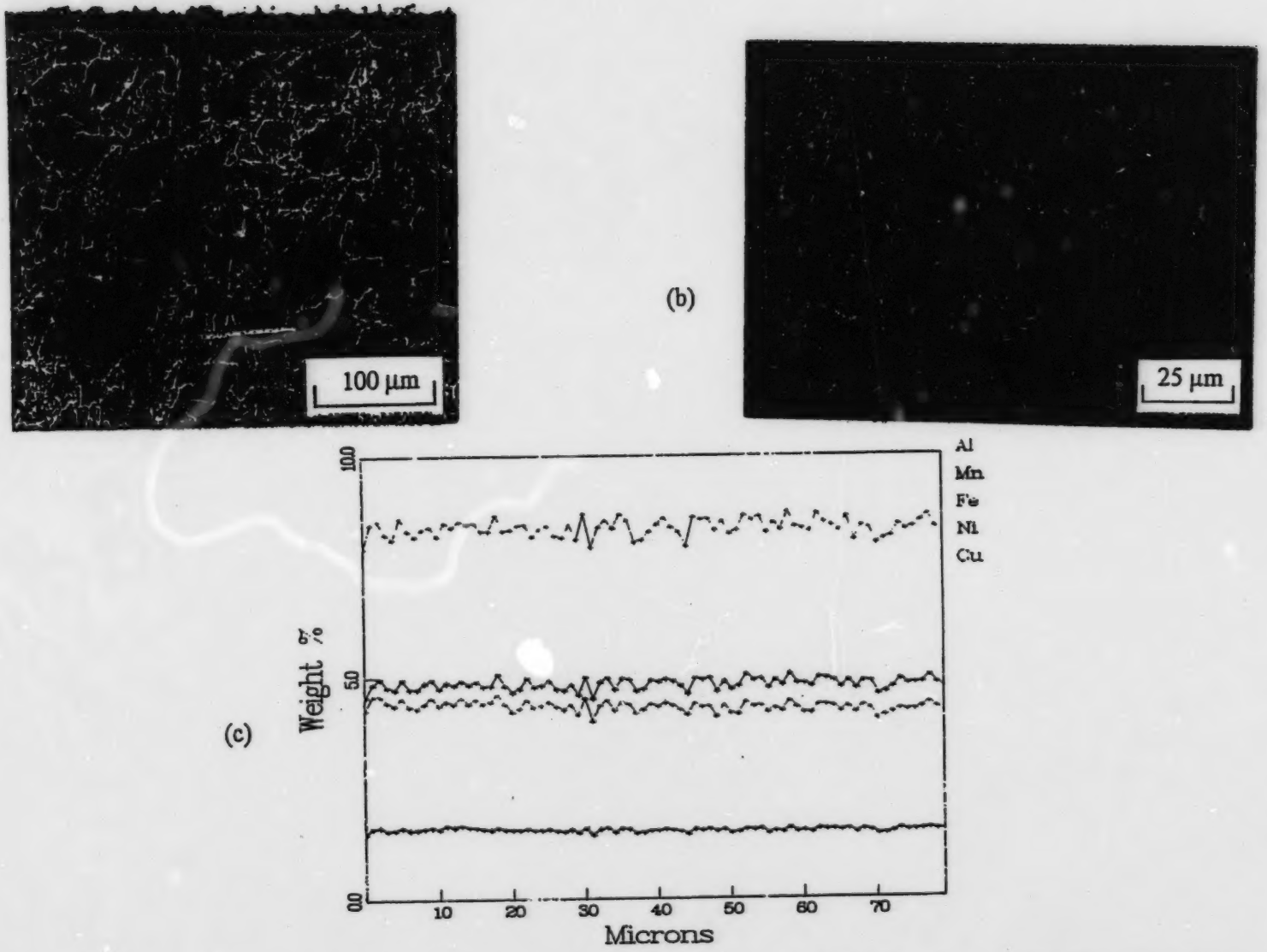

Fig. 10. Optical (a) and SEM back scatter (b) micrographs showing a stage-scan across a predominantly martensitic structure in the as-deposited region and (c) the corresponding concentration profile.

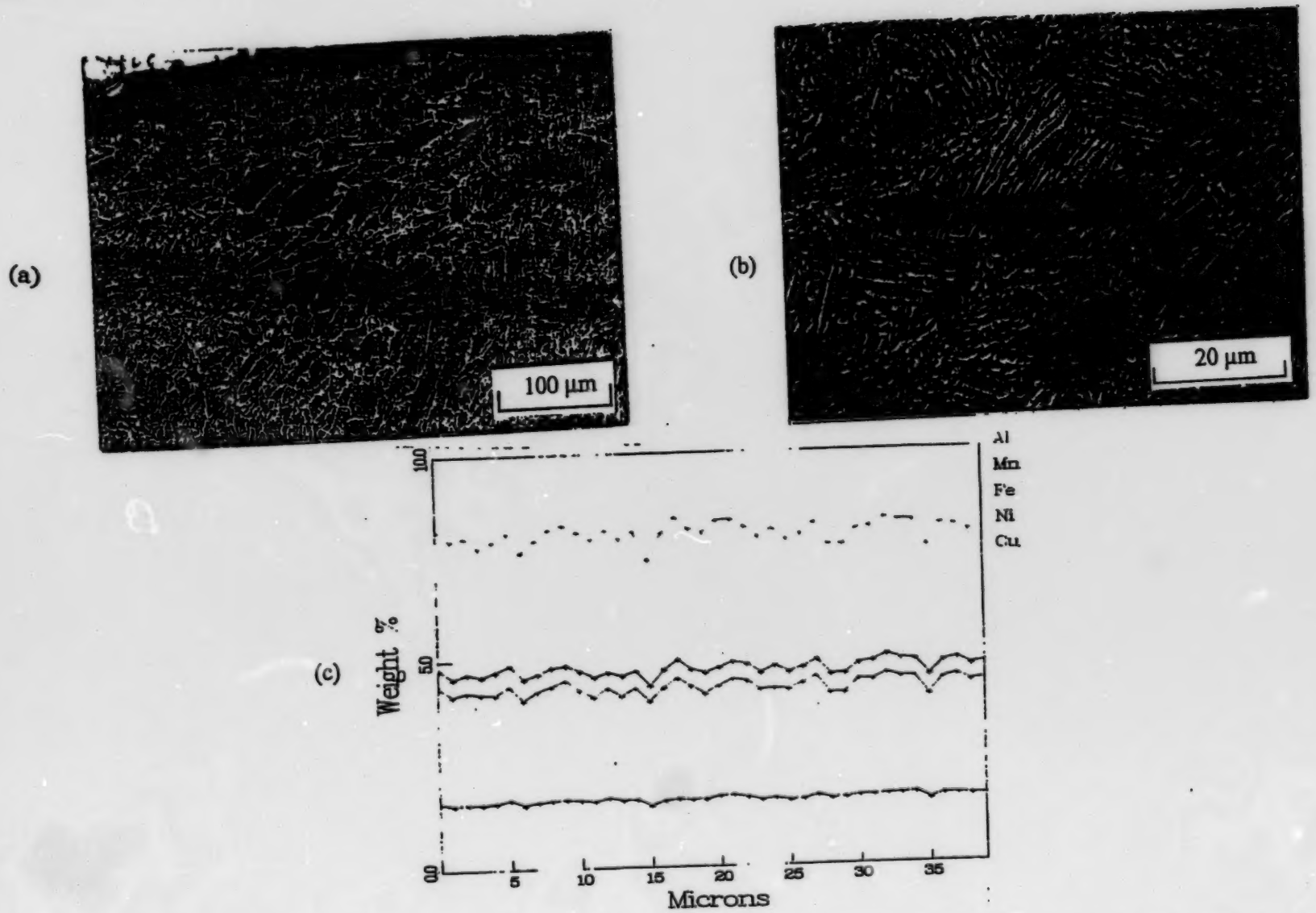

Fig. 11. Optical (a) and SEM back scatter (b) micrographs showing a stage-scan across a Widmanstatten α structure in the as-deposited region and (c) the corresponding concentration profile.

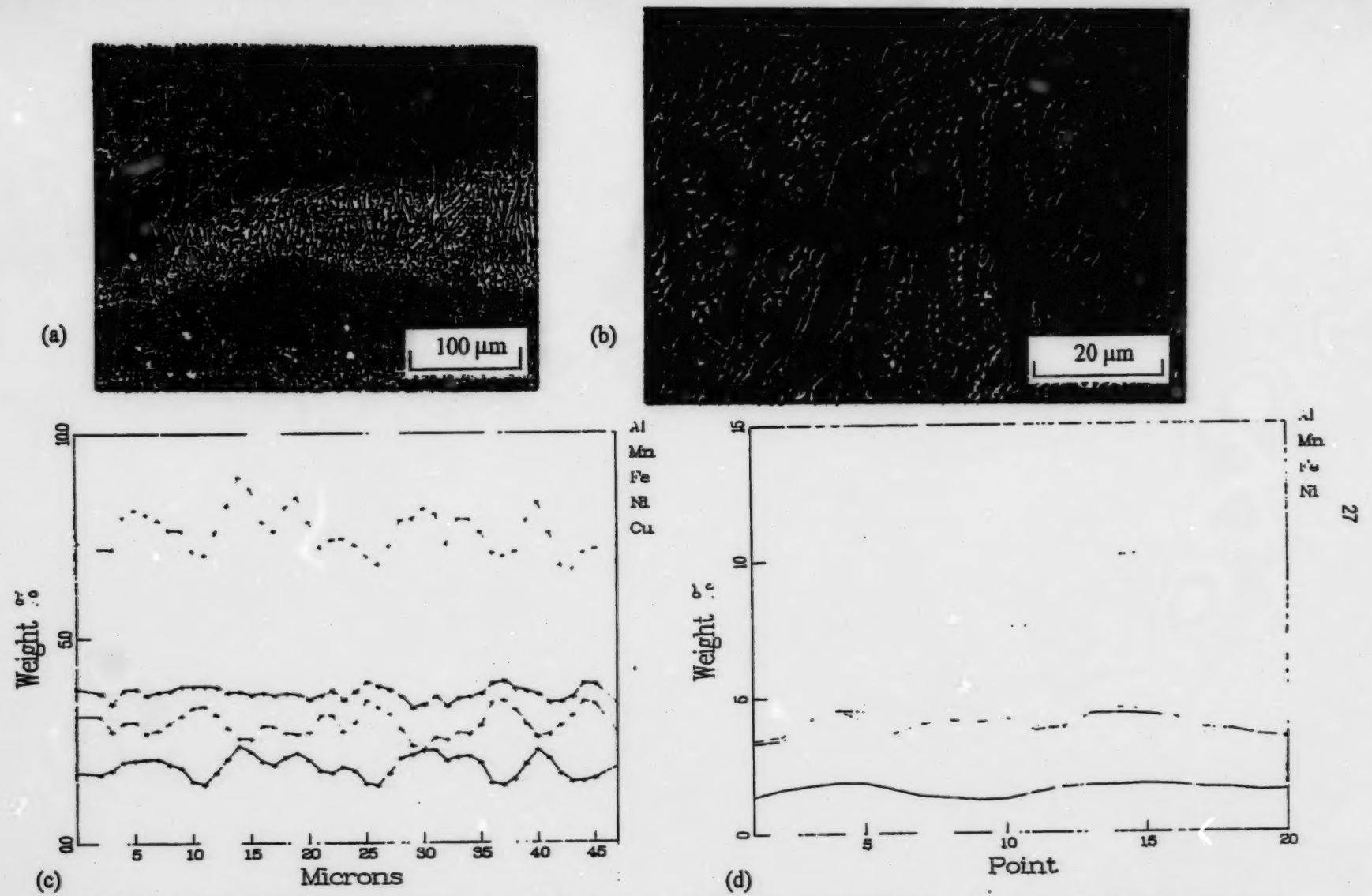

Fig. 12. Optical (a) and SEM back scatter (b) micrographs showing a stage-scan across a dendritic structure near the fusion boundary of the laser clad weld and (c) the corresponding concentration profile. Figure 12(d) is a concentration profile obtained from a similar dendritic structure.

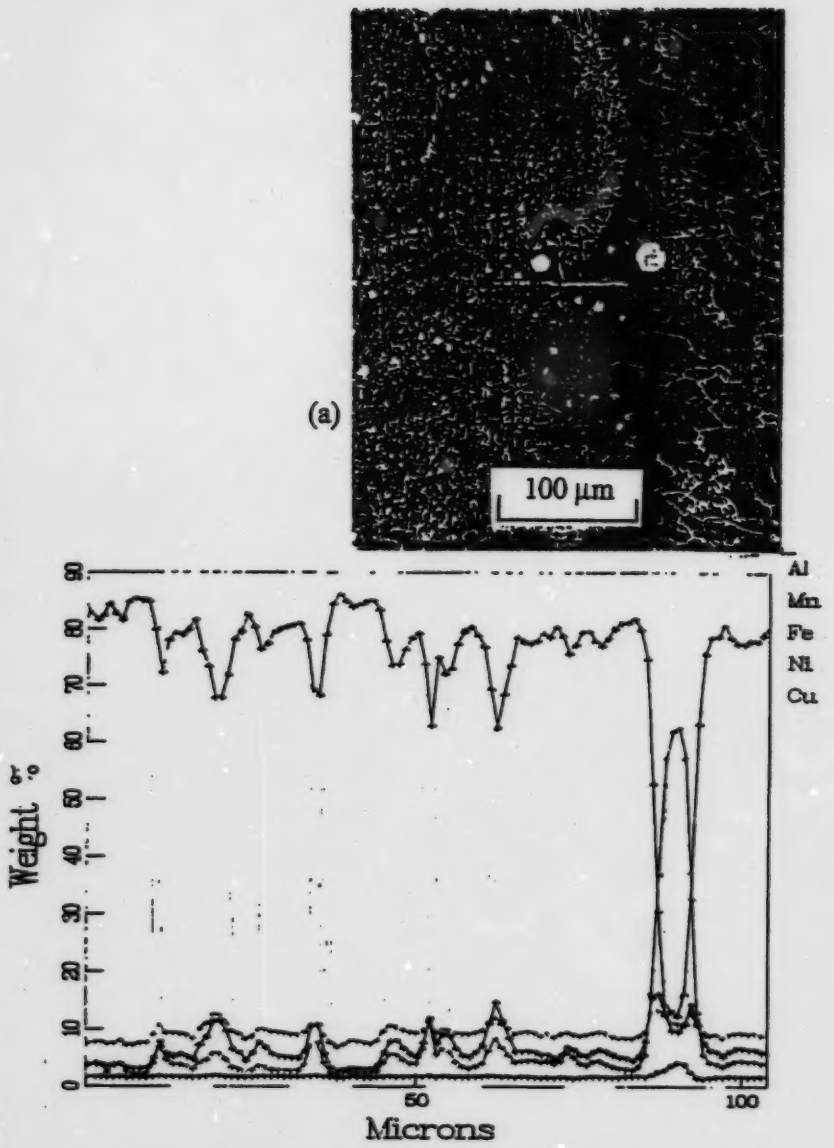

Fig. 13. Optical (a) and SEM back scatter (b) micrographs showing a stage-scan which begins in the HAZ and ends in weld metal just inside the fusion boundary and (c) the corresponding concentration profile.

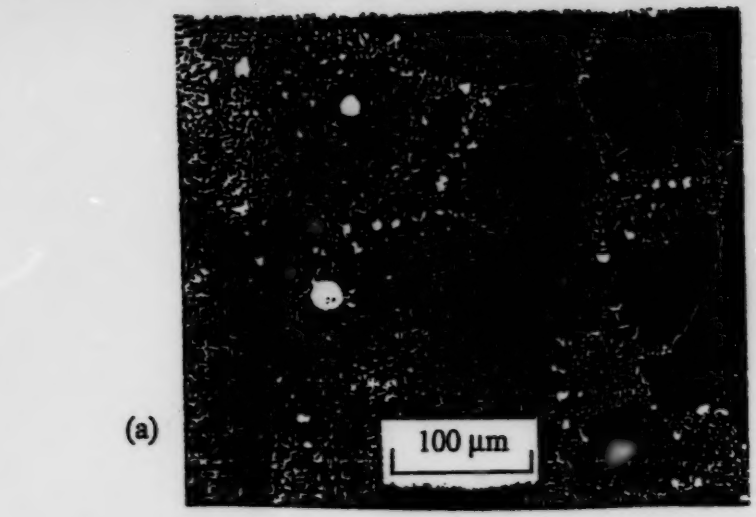

(a)

(b)

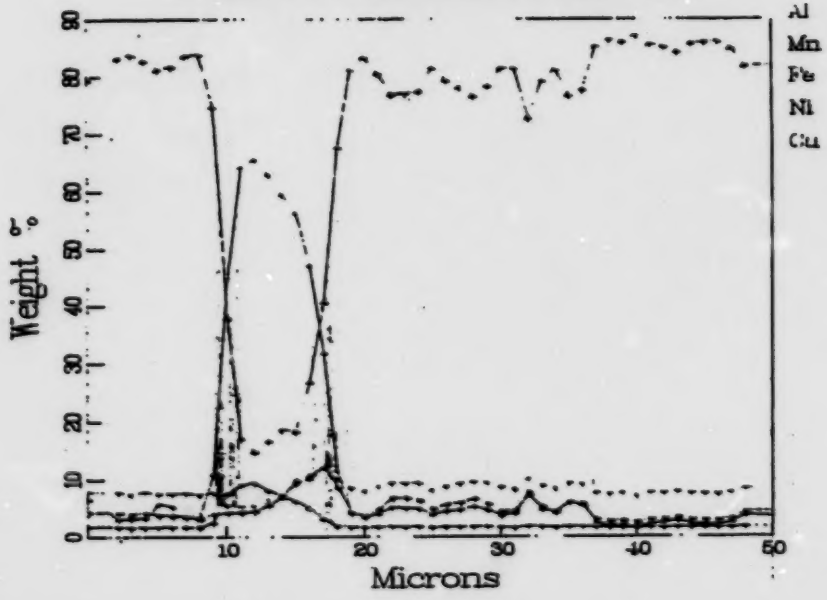

(c)

Fig. 14. Optical (a) and SEM back scatter (b) micrographs showing a stage-scan in the base metal casting which begins in an α grain traverses across a κ_{II} particle, through a eutectoid region, and ends in an adjacent α grain and (c) the corresponding concentration profile.

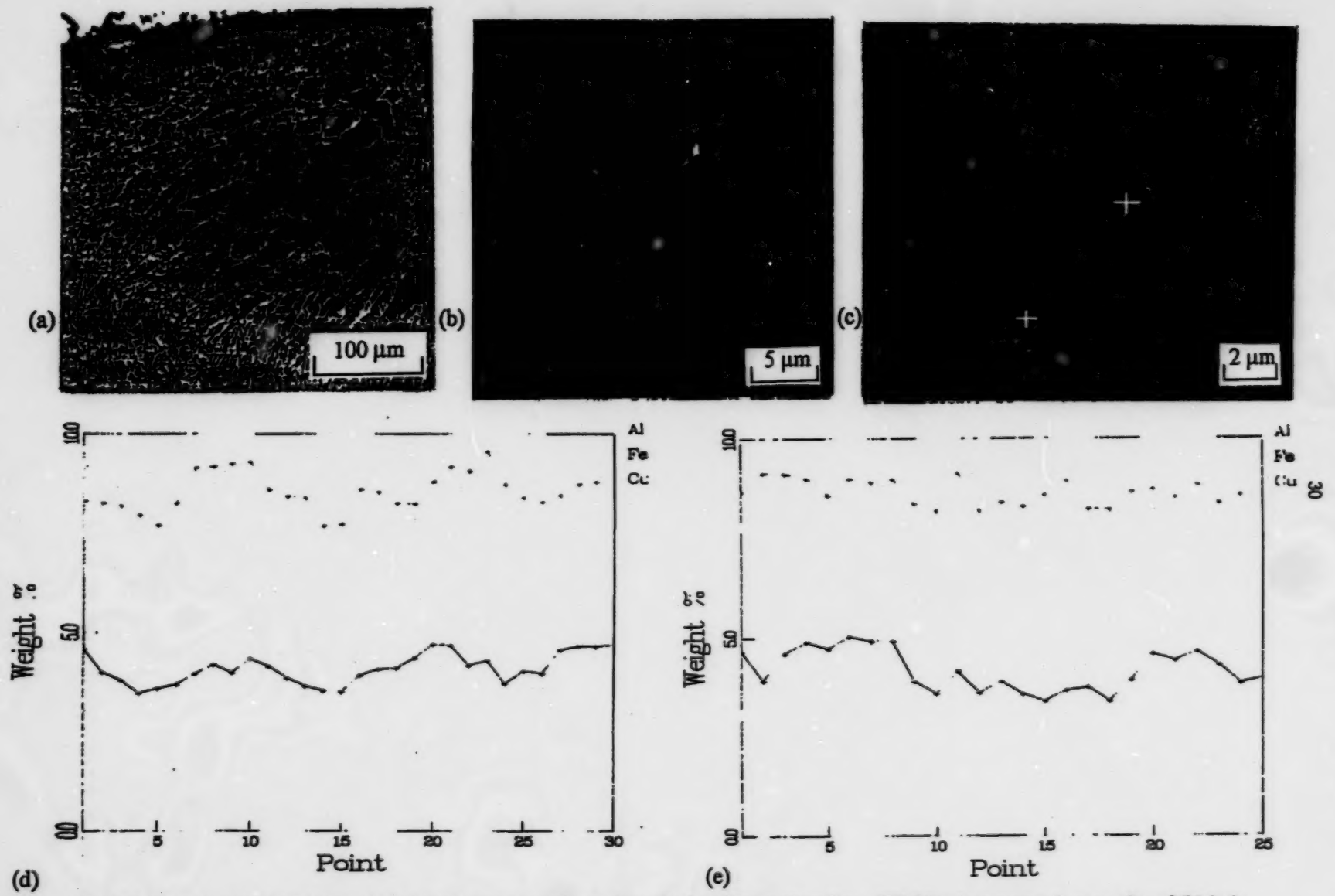

Fig. 15. Optical micrograph (a) showing short beam scans in as-deposited weld metal region. SEM back scatter micrographs of (b) lath structure and (c) martensitic structure and corresponding concentration profiles (d,e).

UNCLASSIFIED
SECURITY CLASSIFICATION OF FORM
(highest classification of Title, Abstract, Keywords)

DOCUMENT CONTROL DATA

(Security classification of title, body of abstract and indexing annotation must be entered when the overall document is classified)

1. ORIGINATOR (the name and address of the organization preparing the document.. Organizations for whom the document was prepared, e.g. Establishment sponsoring a contractor's report, or tasking agency, are entered in section 8.)

Materials Technology Laboratory
CANMET, NRCAN
568 Booth Street, Ottawa, Canada

2. SECURITY CLASSIFICATION (overall security classification of the document including special warning terms if applicable).

UNCLASSIFIED

3. TITLE (the complete document title as indicated on the title page. Its classification should be indicated by the appropriate abbreviation (S,C,R or U) in parentheses after the title).

MICROSTRUCTURAL CHARACTERIZATION AND ELECTRON MICROPROBE ANALYSIS OF A NICKEL ALUMINUM BRONZE LASER-CLAD WELDMENT

4. AUTHORS (Last name, first name, middle initial. If military, show rank, e.g. Doe, Maj. John E.)

J.A. Gianetto, R. Packwood and M. Sahoo

5. DATE OF PUBLICATION (month and year of publication of document)

August 1999

6a. NO .OF PAGES (total containing information include Annexes, Appendices, etc).

33 (approx.)

6b. NO. OF REFS (total cited in document)

7. DESCRIPTIVE NOTES (the category of the document, e.g. technical report, technical note or memorandum. If appropriate, enter the type of report, e.g. interim, progress, summary, annual or final. Give the inclusive dates when a specific reporting period is covered).

CONTRACTOR REPORT

8. SPONSORING ACTIVITY (the name of the department project office or laboratory sponsoring the research and development. Include address).

Defence Research Establishment Atlantic
PO Box 1012
Dartmouth, NS, Canada B2Y 3Z7

9a. PROJECT OR GRANT NO. (if appropriate, the applicable research and development project or grant number under which the document was written. Please specify whether project or grant).

1gh16

9b. CONTRACT NO. (if appropriate, the applicable number under which the document was written).

10a ORIGINATOR'S DOCUMENT NUMBER (the official document number by which the document is identified by the originating activity. This number must be unique to this document.)

10b OTHER DOCUMENT NOs. (Any other numbers which may be assigned this document either by the originator or by the sponsor.)

DREA CR-1999-116

11. DOCUMENT AVAILABILITY (any limitations on further dissemination of the document, other than those imposed by security classification)

(X) Unlimited distribution
( ) Defence departments and defence contractors; further distribution only as approved
( ) Defence departments and Canadian defence contractors; further distribution only as approved
( ) Government departments and agencies; further distribution only as approved
( ) Defence departments; further distribution only as approved
( ) Other (please specify):

12. DOCUMENT ANNOUNCEMENT (any limitation to the bibliographic announcement of this document. This will normally correspond to the Document Availability (11). However, where further distribution (beyond the audience specified in (11) is possible, a wider announcement audience may be selected).

Full Unlimited Announcement

UNCLASSIFIED
SECURITY CLASSIFICATION OF FORM
UNCLASSIFIED
SECURITY CLASSIFICATION OF FORM
(highest classification of Title, Abstract, Keywords)

13. ABSTRACT (a brief and factual summary of the document. It may also appear elsewhere in the body of the document itself. It is highly desirable that the abstract of classified documents be unclassified. Each paragraph of the abstract shall begin with an indication of the security classification of the information in the paragraph (unless the document itself is unclassified) represented as (S), (C), (R), or (U). It is not necessary to include here abstracts in both official languages unless the text is bilingual).

In this study the microstructural and compositional variations that exist across a laser-clad weldment produced with a heat input of 150 J/cm and filler wire composition Cu-9.0% Al, 4.6% Ni, 3.9% Fe and 1.2% Mn were characterized. The weld metal, heat-affected zone and casting base metal structures and elemental distributions were evaluated using light optical microscope and electron microprobe, respectively. The results show that a considerable range of microstructures and some significant compositional variations are present in the laser-clad weldment investigated.

14. KEYWORDS, DESCRIPTORS or IDENTIFIERS (technically meaningful terms or short phrases that characterize a document and could be helpful in cataloguing the document. They should be selected so that no security classification is required. Identifiers, such as equipment model designation, trade name, military project code name, geographic location may also be included. If possible keywords should be selected from a published thesaurus, e.g. Thesaurus of Engineering and Scientific Terms (TEST) and that thesaurus-identified. If it not possible to select indexing terms which are Unclassified, the classification of each should be indicated as with the title).

Nickel Aluminum Bronze
Cladding
Laser
Welding
Electron microprobe
Metallography
Composition variations